

Microsphere-based cantilevers for polarization-resolved and femtosecond SNOM

C. A. González Mora¹ · M. Hartelt¹ · D. Bayer¹ · M. Aeschlimann¹ · E. A. Ilin² · E. Oesterschulze²

Received: 15 August 2015 / Accepted: 6 February 2016 / Published online: 6 April 2016
© Springer-Verlag Berlin Heidelberg 2016

Abstract We present a cantilever-based near-field probe with integrated Mie scattering dielectric SiO₂ microsphere (MSDM) for near-field optical imaging as well as femtosecond spectroscopy applications. In contrast to the state-of-the-art transmissive near-field probes, the MSDM reveals a transmission of almost unity known from far-field microscopy configuration. For proper handling, the microsphere is integrated at the apex of a conventional pyramidal aperture tip carried by an atomic force microscopy cantilever. It proved to be mechanically robust during the scanning process even if operating it in the contact mode. The spherical symmetry provides on the one hand a well-defined mechanical contact point with the sample irrespective of its inclination angle to the sample surface. On the other hand, the symmetry of the device preserves the polarization of light proving to be useful for the investigation of the polarization dependent behavior of plasmonic nanostructures. The high transmission combined with low dispersion renders spectroscopic investigations on the femtosecond timescale with a moderate lateral resolution. Second order autocorrelation experiments on a BBO crystal

reveals a time resolution well below 100 fs at 191 nm spatial resolution.

1 Introduction

The concept of near-field microscopy with nanoaperture based probes has been under continuous evolution since the first realization by Pohl et al. in the early 1980s [1]. The probe design has evolved from tapered fibers made by the pulling and heating method [2] to chemically etched fibers [3] and later on to atomic force microscopy cantilever probes with integrated hollow pyramidal tips [4, 5]. Common to all these probes is a light-guiding metallized tapered waveguide with a tiny aperture at its end. For apertures distinctly smaller than the wavelength of light, the lateral resolution outperforms that of conventional microscopes. However, there are still important drawbacks like the extreme low transmission (e.g., 10⁻⁶ for an aperture of 100 nm [6]). The metal grains that define the rim of the aperture affect the polarization and emission characteristics and thus may modify the near-field optical signal [7].

In the first transition, from pulled fibers to etched ones, the main goal was to improve the reproducibility and the throughput of the device by tuning the angle of the fiber, leading to the enhancement of the transmission through the aperture. However, the microscopical roughness of the walls of the fiber was the main problem which was reduced by the method of tube etching [8]. On the other hand, the design of probes based on atomic force cantilevers consists of a pyramid with fourfold symmetry made of a thin SiO₂ or SiN layer coated with a thin aluminium layer to avoid light leakage. The dimension of apertures was typically in the order of 100 nm diameter. Their large opening angle of approx. 70° substantially reduced the taper length and thus

This article is part of the topical collection “Ultrafast Nanooptics” guest edited by Martin Aeschlimann and Walter Pfeiffer.

✉ C. A. González Mora
mora@rhrk.uni-kl.de

E. Oesterschulze
oester@physik.uni-kl.de

¹ Department of Physics and Research Center OPTIMAS, University of Kaiserslautern, Erwin Schroedinger Str. 46, 67663 Kaiserslautern, Germany

² Department of Physics, Physics and Technology of Nanostructures, University of Kaiserslautern, Erwin Schroedinger Str. 46, 67663 Kaiserslautern, Germany

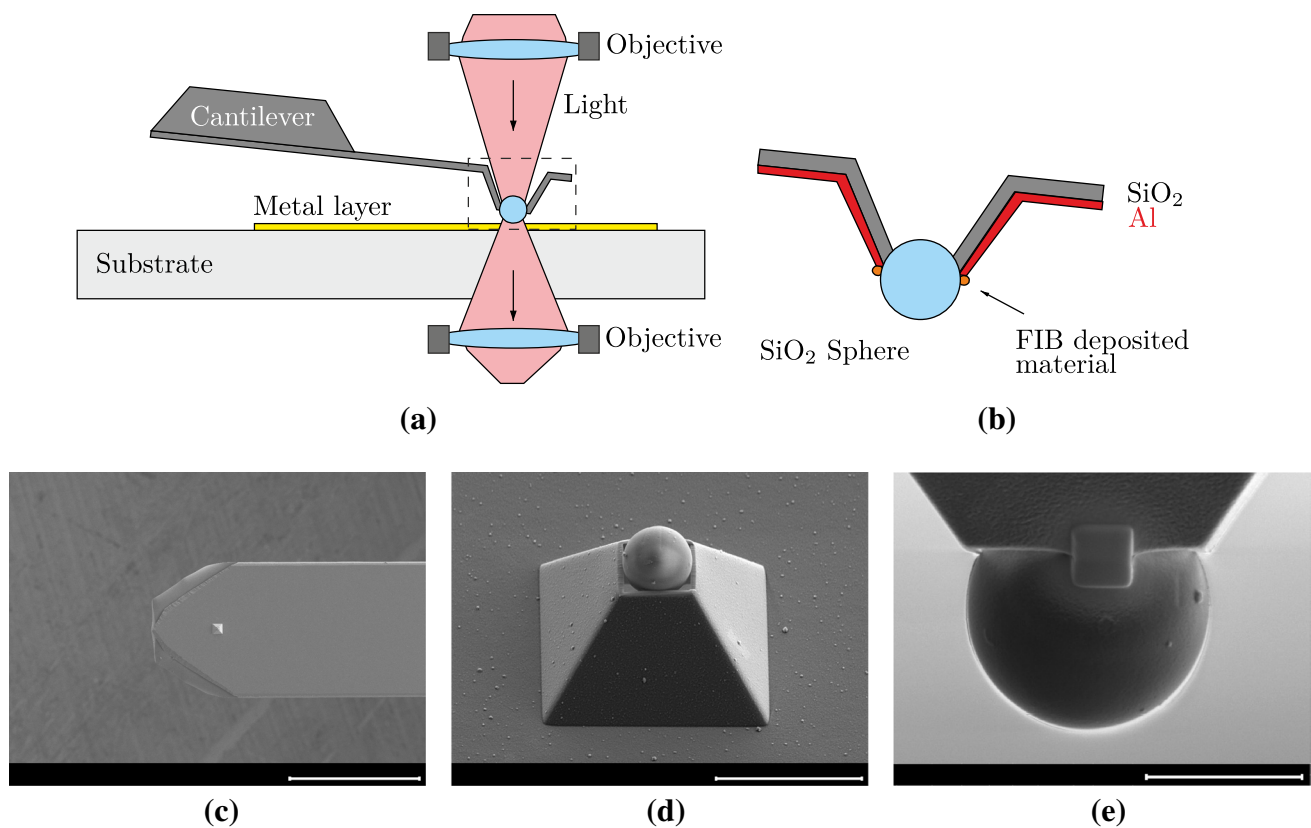


Fig. 1 **a** Scheme of the near-field cantilever probe installed into a transmission microscope. **b** Cross section of the hollow tip showing the dielectric microsphere clamped at the rim of the aperture. Scanning electron microscope (SEM) images of **c** the cantilever (scale

bar 200 μm), **d** the hollow tip (scale bar 10 μm) and **e** a fixed sphere (scale bar 3 μm). To withstand larger forces during the scanning process, the microsphere was fixed by ion-assisted deposition of a small spot of Pt-C material at the rim of the aperture

improved the throughput with respect to the fiber based probes [9]. Although microfabrication techniques were utilized for manufacturing, the reproducibility of the aperture still is an issue due to the aperture-opening process. The aperture that is expected to be round and placed exactly at the apex of the pyramid often reveals merely an elliptical shape and sometimes is shifted tens of nanometers out of the apex position introducing additional polarization pinning effects [10]. Due to these issues, every single pyramidal tip is still unique and has only limited reproducible properties. Even though this structure is robust and capable to endure the mechanical stress applied to keep it in contact with the sample, it is not rigid enough to withstand abrasion during ongoing scanning processes in the near-field microscope. For this reason, a single cantilever probe can practically not be used for more than a single scan without affecting its lateral resolution.

In this paper, we present a new type of cantilever for near-field optics with a Mie scattering dielectric microsphere as sensing part integrated into the hollow pointed tip of a cantilever, Fig. 1a. This imaging scheme based on scattering dielectric microspheres for near-field optics

was first introduced by Wang et al. and was named “nanoscope” [11]. It was successfully applied for parallel imaging of 50 nm objects in a conventional microscope dispensing microspheres randomly onto the sample surface. Using white light from a halogen lamp with a peak wavelength at $\lambda = 600$ nm, they were capable to surpass the diffraction limit of far-field microscopy [11]. One of the beneficial features of such a device is the capability of the microsphere to focus light on areas smaller than at least half the wavelength providing simultaneously an excellent transmission which is comparable to that of conventional microscope set-ups. This renders their application for femtosecond (fs) spectroscopy with improved spatial resolution possible. In contrast to nanoscopy, fs experiments require to consecutively gather optical information point by point while scanning the probe across the sample to establish temporal image formation.

2 Design and construction of the probes

For practical applications in a near-field microscope, it is necessary to integrate the Mie scattering dielectric

microsphere into a mechanical holder that allows to address a certain position on the sample surface [12]. Therefore, we have fabricated atomic force microscopy cantilever probes with an integrated hollow pyramidal tip following the process described in [4]. In detail, the hollow pointed tip consists of a 300 nm thin silicon dioxide layer coated by a 200 nm Al film to block the optical transmission through the four side walls of the pyramid. For the installation of a single microsphere (Bang laboratories, silica spheres with diameters: 4.5, 2.5 and 1.2 μm), the pyramidal tip was opened by slicing it from the side by focused ion beam milling (FEI Helios 650). The size of the aperture was chosen to be roughly 100 nm smaller than the diameter of the desired sphere. The microsphere attachment to the tip was initiated by dropping a dilute solution of the sphere dispersion onto a glass slide. After drying, most of the attached microspheres were removed in a nitrogen gas stream to ensure that enough free-lying spheres were available for installation. Then the glass slide was installed into a modified commercial scanning near-field optical microscope (α -SNOM, WiTeC), see Fig. 2. Illumination from the top allowed to identify a certain sphere on the surface with a CCD camera. The stage of the microscope was positioned such that the sphere was centered exactly on the screen. Afterward the same sphere was imaged from the bottom with an objective and a second CCD camera catching up all the light transmitted through the microsphere. The image was also centered on the screen by moving the bottom objective with a 3D stage. Later on, the cantilever with the sliced tip was positioned with a 3D micromanipulator stage (Kammrath and Weiss) from the top while

centering the tip exactly above the desired sphere. For large distances between tip and microsphere, the light was sufficiently obstructed by the tip. While approaching the cantilever in z -direction with the stage, the transmitted intensity through the sphere increased when continuously centering the tip and aperture by the motion of the xy -stages carrying the cantilever. To avoid any mechanical damage of the tip, the approach was ceased when the light transmitted through the sphere was almost at the original intensity obtained without cantilever. By then retracting the cantilever tip in z -direction in most cases the sphere adhered to the rim of the aperture finalizing the MSDM. However, AFM contact mode experiments revealed that adhesion was not always sufficient because there are only four contact points between the rim of the square aperture and the sphere. Therefore, we deposited a roughly 200 nm dot of a Pt-C compound by ion assisted chemical vapor deposition in the FIB at one side of the aperture rim to fix the microsphere reliably, see Fig. 1e. The presence of the Pt-C compound did not show any undesirable optical signal since it is located in the region shaded by the Al coating of the pyramid which avoids the direct illumination by the laser.

3 Experimental results

The optical performance of the sensors was investigated imaging plasmonic nanostructures with the main attention on three properties: transmission, spatial resolution, and the preservation of the near-field polarization. The sample itself consisted of a two-dimensional array of rings made from a stack of a 40 nm gold layer deposited onto a 100 nm 100 nm indium tin oxide (ITO) coated glass substrate. In each row of the array, the inner radius was systematically increased going from left to right for a preserved outer radius while in each column the outer radius was decreased from top to bottom for a given inner radius. This sample configuration was chosen because of its almost negligible topography but also because it supports the excitation of localized surface plasmons (LSPs) at certain wavelengths for an adapted ring geometry.

Prior to each near-field measurement, the intensity of the light needed to be reduced and adjusted to avoid saturation of the photomultiplier tube used to amplify measured signal. The saturation is a consequence of the huge transmission of the MSDM that is almost unity [12]. After this adjustment, the metal ring structures were first investigated in the off-resonance regime at a wavelength of 532 nm using a microsphere with a diameter of 4.5 μm . The optical transmission measurements were performed in contact with the surface at a speed of 5 $\mu\text{m/s}$. In the measurement shown in Fig. 3b, the structures are visible as dark rings corresponding to a decrease in the transmission due to the

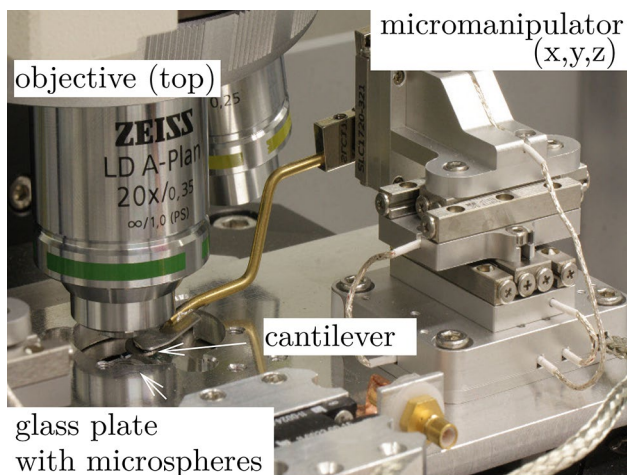


Fig. 2 Image of the set-up used for the mounting process of the microspheres: A three-dimensional translational micromanipulator with a mechanical brass holder is used to position the cantilever's tip atop a single sphere on the glass slide. The microsphere is picked up by moving the cantilever downwards clamping the sphere into the slightly smaller aperture of the tip

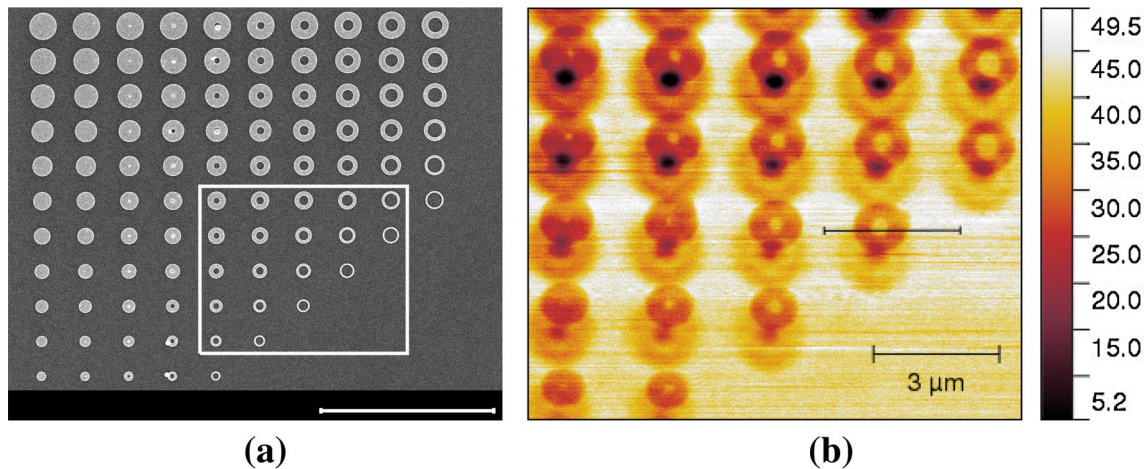


Fig. 3 **a** SEM image of the sample consisting of an array of Au ring structures (scale bar $10\ \mu\text{m}$). **b** SNOM image taken at a wavelength $\lambda = 532\ \text{nm}$, the scanned area corresponds to the frame indicated in **a** and the scale bar represents intensity in hundreds of counts by a PMT

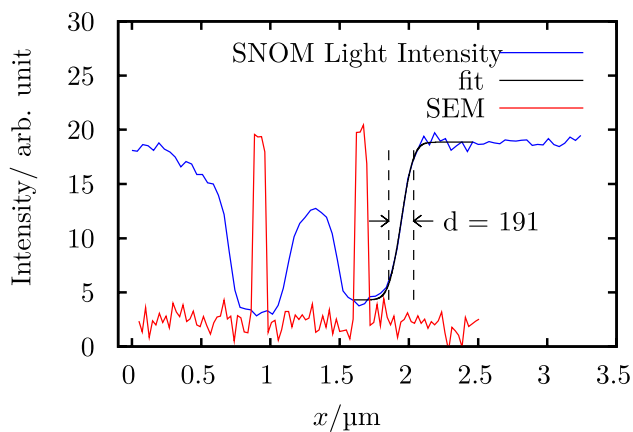


Fig. 4 Line scans through a SEM image (red) and the corresponding SNOM measurements (blue) taken at the marked position in Fig. 3b

presence of the ring. We also observed vertically displaced shadow rings of lower contrast whose origin is not yet identified. From line scans across the measured ring structures, a moderate lateral resolution of $191\ \text{nm}$ (roughly $\lambda/2.8$) was deduced applying the 10–90 % criterion, see Fig. 4. This is larger than the resolution of ca. $150\ \text{nm}$ that we obtained with conventional aperture cantilevers. Further optimization of the lateral resolution can probably be achieved by varying the size and material of the microspheres in order to reduce the size of the focus [11].

4 Simulations

Numerical simulations were performed with a commercial software (FDTD Solutions v.8.12.527, Lumerical Solutions Inc.) in order to compare them with the experimental

results. The software uses the finite difference time domain (FDTD) method combined with an automatic meshing algorithm to generate a non-uniform mesh considering the material properties and geometry of the simulated region. The underlying simulation geometry consists of a SiO_2 ($n = 1.45$) sphere of $4.5\ \mu\text{m}$ diameter on a glass substrate ($n = 1.45$) extended further than the simulation boundaries. Illumination was performed with a plane wave propagating in the z -direction normal to the surface of the glass plate and with the polarization parallel to the x -axis. Perfectly matched layer (PML) boundary conditions were chosen to minimize the influence of reflections coming from the boundaries of the simulation region. From these simulations, intensity distribution and profiles were extracted for the desired wavelengths.

From the simulations, the first noticeable feature is the capability of the sphere to focus the light at the surface of the glass plate as it was already discussed by Wang et al. [11]. In Fig. 5a, the slice of the intensity distribution for the vertical plane through the center of the sphere and perpendicular to the substrate is depicted, in which the focusing effect at the surface of the glass plate at $532\ \text{nm}$ excitation wavelength is clearly visible. The $I_x = |E_x|^2$ intensity distribution near the surface of the glass substrate is depicted in Fig. 5b, while $I_z = |E_z|^2$ is depicted in Fig. 5c. From both slices as well as from the overall intensity $I = |\mathbf{E}|^2$, line scans at $y = 0$ were extracted as are shown in Fig. 5d.

An estimation of the focal size of the total intensity distribution at the sample surface revealed a size of about $750\ \text{nm}$ which is 1.5 times the wavelength. This observation is in particular contrast to our experimental findings in Fig. 4 that reveals a lateral resolution of ca. $190\ \text{nm}$. To understand this discrepancy, we first took a closer look

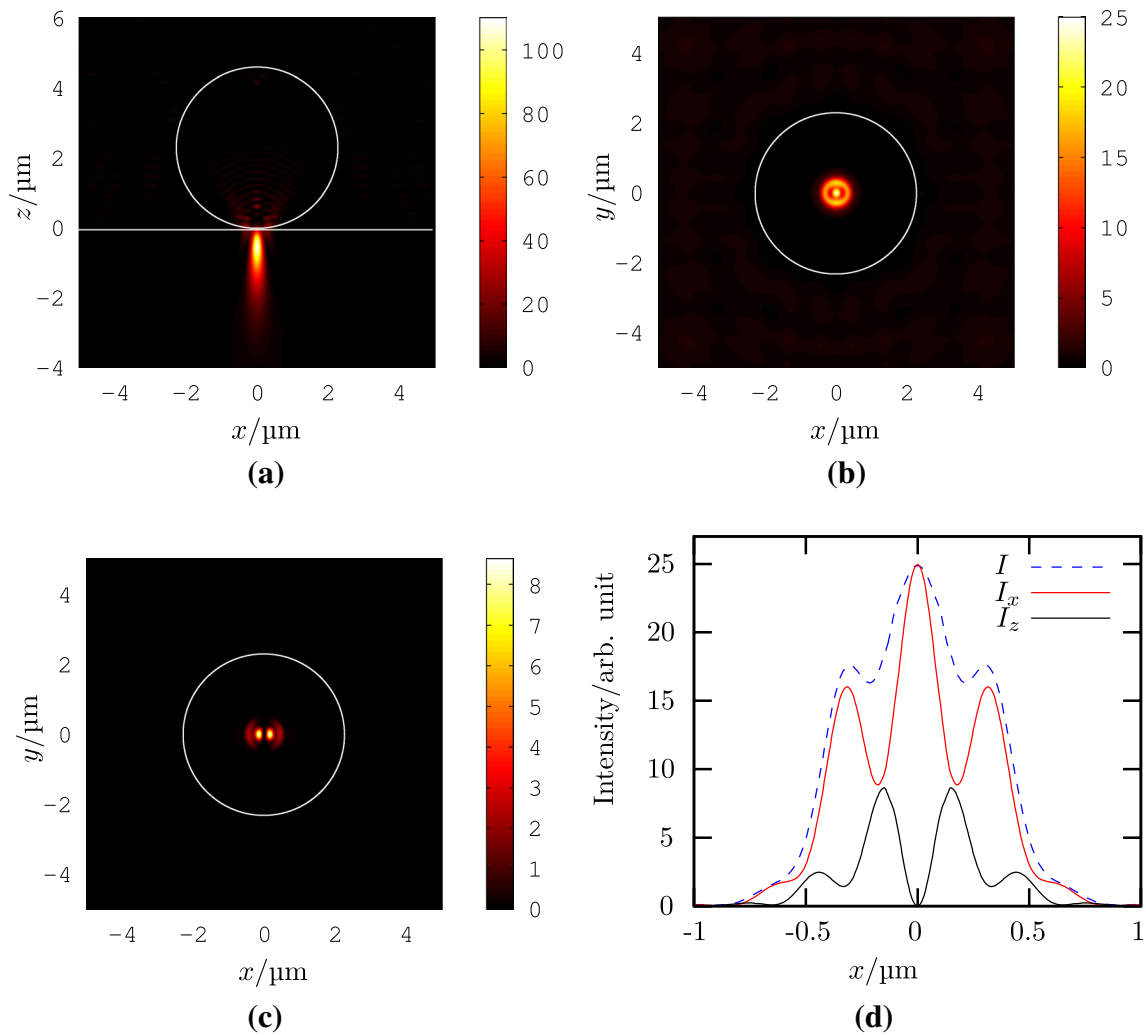


Fig. 5 Images of the simulated intensity distribution for a 4.5 μm diameter sphere on a glass substrate at 532 nm illumination wavelength. **a** Cut of the electric field intensity I at the xz -plane at $y = 0$ (through the center of the sphere, normal to the substrate and paral-

lel to the polarization direction), **b** cut of the I_x parallel through the substrate (xy -plane) at $z = -20$ nm under the sphere, **c** cut of I_z in the same plane as for **(b)**, **d** intensity profile from $y = 0$ in **(b)** and **(c)**

at the intensity profiles of the field components in x - and z -directions. The y -component of the electric field was by two orders of magnitude smaller and is neglected in the following discussion. The profile of I_x , the field along the polarization direction of the incident plane wave, resembles that of the total intensity, showing a central maximum with symmetric side lobes as expected from Mie theory of dielectric spheres. However, the size of the maxima is still in the order of $\lambda/2$ at best. On the other hand, for the z -component, we see two maxima with a FWHM of about 150 nm separated by a cross point. Each of the lobes is moved across the sample structure while scanning the probe. This suggests, at first glance, that the observed resolution in the image is presumably affected by the strong variation of E_z which is only by a factor of two smaller than E_x . However, Wang et al. [11] have already investigated and discussed

the impact of dielectric Mie scattering spheres on the imaging process. They were capable to show that in the presence of the scattering sphere, a virtual magnified image forms below the sample surface if the radius and refractive index of the sphere is chosen appropriately. A detailed understanding of the microscopic interaction mechanism of the dielectric sphere and the gold ring pattern demands a much more intricate and thorough theoretical modeling, which is beyond the scope of this paper.

In the case of wavelengths in the range of 780–820 nm, covering the wavelength regime of a Ti:Sapphire oscillator with pulses as short as ~ 25 fs, the size of the focus is almost constant. From Fig. 6a, a focus width of 530 nm is determined from the total intensity distribution with a variation smaller than 10% as shown in Fig. 6b. Images of the intensity distribution along the x -axis for I_x (Fig. 6c) and I_z

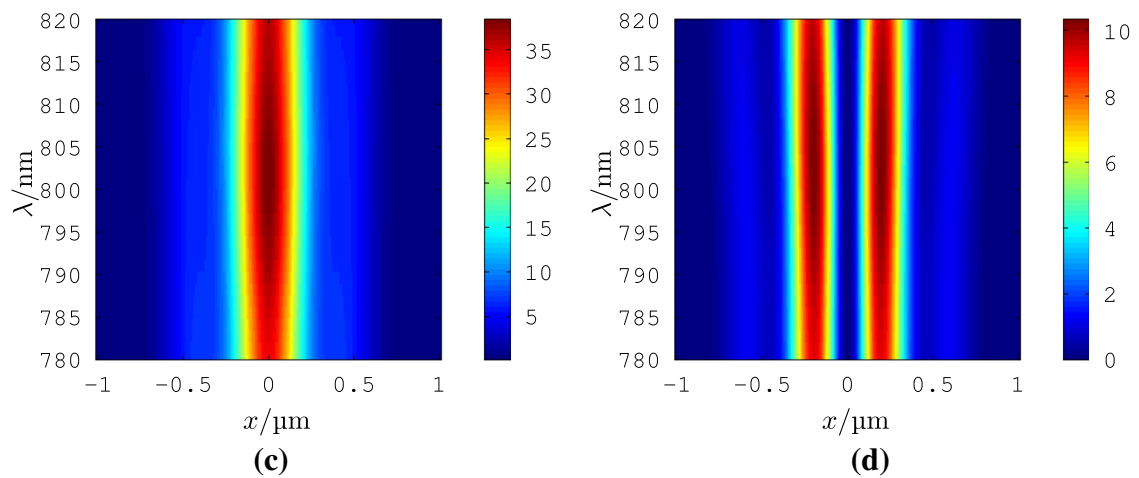
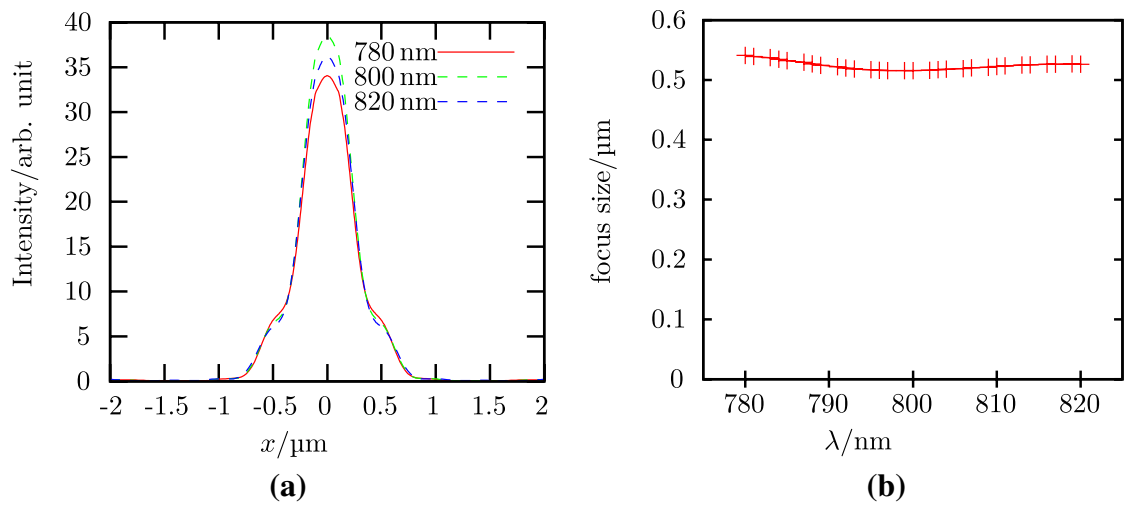
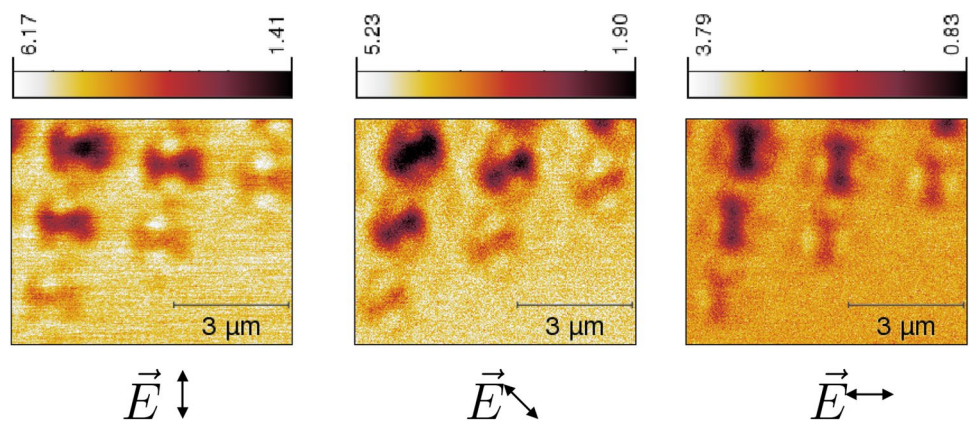


Fig. 6 Images of the simulations of the intensity distribution for a $4.5\ \mu\text{m}$ diameter sphere on a glass substrate around $800\ \text{nm}$ illumination wavelength. **a** Intensity I profiles in the xy -plane at $z = -20\ \text{nm}$ for different wavelengths, **b** plot of the focal size (FWHM) for I_x as

function of the wavelengths in the xy -plane at $z = -20\ \text{nm}$ under the sphere. Stack of intensity profiles for **c** E_x and **d** E_z in the range $x \in [-1, 1]\ \mu\text{m}$ for different wavelengths at $y = 0$

Fig. 7 SNOM measurements of ring resonators in resonance at $\lambda = 800\ \text{nm}$ for different polarization directions: vertical, diagonal, and horizontal. Scale bars represent intensity in hundreds of counts by a PMT



(Fig. 6d) as function of the wavelength show only minor variations of the focal size which is beneficial for the focusing of ultrafast pulses through dielectric spheres.

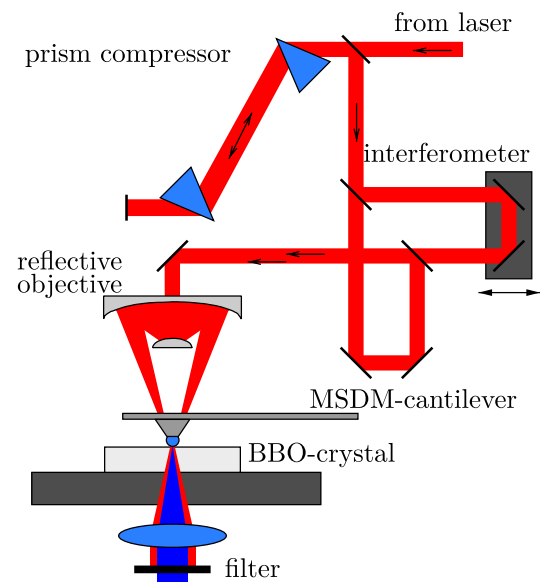
5 Application for plasmonics and time-resolved measurements

The benefits of the new probes got apparent when exciting localized plasmons using the linearly polarized light of a Ti:Sapphire oscillator at 800 nm for excitation. For such Au rings, a dipolar excitation parallel to the polarization of the beam is expected and revealed by the field enhancement due to the localized plasmons as it has been studied in [13, 14]. The polarization of the incoming laser beam was additionally turned with a $\lambda/2$ retarding plate to investigate the impact of the probe on the polarization state at the sample surface.

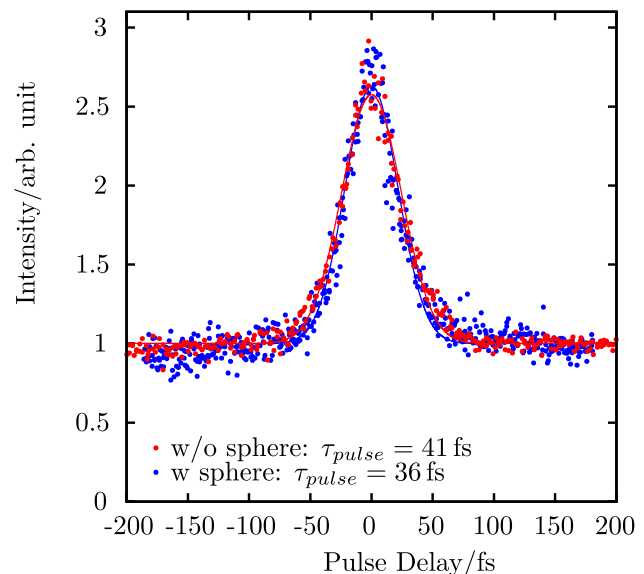
The measurements confirmed the dipolar excitation on the rings revealed by the enhancement of the field distribution with respect to the background signal, see Fig. 7. When turning the polarization of the incoming light, the pattern of the dipolar plasmonic response exactly follows the direction of the polarization. This is due to the high symmetry of the dielectric sphere used as Mie scattering probe.

The high optical throughput of the probes is a rudiment to apply scattering microspheres in the field of fs spectroscopy combined with high lateral resolution. As a proof of principle, we studied the nonlinear process of second harmonic generation (SHG) by a β barium borate (BBO) crystal. For this experiment, the set-up was extended to a pump-probe experiment where laser pulses were split by a Mach-Zehnder interferometer as depicted in Fig. 8a and, finally, recombined introducing a time delay between the two pulses. The goal was to obtain the phase-integrated second-order autocorrelation curve (ACC) and, therefore, the temporal length of the pulses after passing the sphere.

In order to determine the role of the scattering sphere with its intrinsic dispersion on the signal, we compared ACC measurements with and without optical probe. In the first case, the laser was focused through the MSDM-cantilever onto the BBO crystal while in the second case the laser was focused directly onto the crystal. From the respective measurements of the ACC, the pulse duration was deduced from the full width at half maximum of a Gaussian fit. The pulse duration obtained from the ACC of free propagating beam was 41.0(7) fs and for the system with the MSDM-cantilever was 36.0(7) fs. To reach such a pulse length, it was necessary to implement a prism compressor to pre-compensate for the second-order dispersion introduced to the pulses by transmission optics inside the microscope [15]. However, corrections to higher-order dispersion, that require a pulse shaper, were not performed.



(a)



(b)

Fig. 8 **a** Diagram of the set-up used to measure the ACC. **b** ACC traces of the measurements with (blue) and without (red) MSDM-cantilever

Some experiments discussed in literature have shown already that the pulse duration through aperture probes is not strongly affected by the near-field tip itself. The pulse length after propagation through the aperture probe was as short as 30 fs for pyramidal cantilevers with apertures in the range of 70 nm [16, 17], and 100 fs for apertures in the range of 100 nm for fiber probes [6]. However, these aperture probes have the same deficiency in common originating from the cut-off effect of the waveguiding probe: the extreme

low transmission of approximately 10^{-5} – 10^{-6} for the above addressed aperture dimensions. This limits their application because of the given damage threshold value of these aperture probes which is in the range of few tens of mW. This is quite different for the Mie scattering microsphere probes because there is no Joule heating of metal structures as in case of aperture tips.

6 Summary

We presented the proof of principle of a new design of a Mie scattering dielectric microsphere probe used for near-field imaging. The microsphere was integrated into a cantilever tip for the ease of handling and proved to be mechanically extremely rigid with respect to abrasion when in contact to the sample. The high symmetry of the probe is advantageous with respect to a well-defined contact geometry with the sample that is irrespective of the cantilever's chosen inclination angle. Although the lateral resolution of $\lambda/2.8$ is moderate, the probe offers advantages properties like the preservation of the polarization on passing through the microsphere as well as its extreme large throughput. The latter property was exploited for optical nonlinear time-resolved autocorrelation experiments on a BBO crystal. This gives the freedom to combine good lateral resolution with excellent time resolution in the same probe.

Acknowledgments We thank the German Science Foundation (DFG) for financial support of the projects OE220/9-2 and AE19/22-2 which were part of the priority program 1391 ultrafast nanooptics. The technical and scientific support by the on-campus Nano Structuring Center (NSC) is kindly acknowledged. C. A. González Mora also wants to thank Mirko Cinchetti, the lecturer on scientific writing at TU Kaiserslautern, for his ongoing support.

References

1. D.W. Pohl, W. Denk, M. Lanz, Optical stethoscopy: Image recording with resolution $\lambda/20$. *Appl. Phys. Lett.* **44**(7), 651 (1984)
2. G.A. Valaskovic, M. Holton, G.H. Morrison, Parameter control, characterization, and optimization in the fabrication of optical fiber near-field probes. *Appl. Opt.* **34**(7), 1215–1228 (1995)
3. P. Hoffmann, B. Dutoit, R.-P. Salathé, Comparison of mechanically drawn and protection layer chemically etched optical fiber tips. *Ultramicroscopy* **61**(1–4), 165–170 (1995). (Selected Papers from the 3rd International Conference on Near-Field Optics and Related Techniques)
4. S. Münster, S. Werner, C. Mihalcea, W. Scholz, E. Oesterschulze, Novel micromachined cantilever sensors for scanning near-field optical microscopy. *J. Microsc.* **186**(1), 17–22 (1997)
5. N.F. van Hulst, M.H.P. Moers, B. Bölger, Near-field optical microscopy in transmission and reflection modes in combination with force microscopy. *J. Microsc.* **171**(2), 95–105 (1993)
6. B.A. Nechay, U. Siegner, M. Achermann, H. Bielefeldt, U. Keller, Femtosecond pump-probe near-field optical microscopy. *Rev. Sci. Instrum.* **70**(6), 2758–2764 (1999)
7. B. Hecht, B. Sick, U.P. Wild, V. Deckert, R. Zenobi, O.J.F. Martin, D.W. Pohl, Scanning near-field optical microscopy with aperture probes: fundamentals and applications. *J. Chem. Phys.* **112**(18), 7761 (2000)
8. R. Stöckle, C. Fokas, V. Deckert, R. Zenobi, B. Sick, B. Hecht, U.P. Wild, High-quality near-field optical probes by tube etching. *Appl. Phys. Lett.* **75**(2), 160 (1999)
9. A. Vollkopf, O. Rudow, T. Leinhos, C. Mihalcea, E. Oesterschulze, Modified fabrication process for aperture probe cantilevers. *J. Microsc.* **194**(2–3), 344–348 (1999)
10. P. Biagioni, D. Polli, M. Labardi, A. Pucci, G. Ruggeri, G. Cerullo, M. Finazzi, L. Duò, Unexpected polarization behavior at the aperture of hollow-pyramid near-field probes. *Appl. Phys. Lett.* **87**(22), 223112 (2005)
11. Z. Wang, W. Guo, L. Li, B. Luk'yanchuk, A. Khan, Z. Liu, Z. Chen, M. Hong, Optical virtual imaging at 50 nm lateral resolution with a white-light nanoscope. *Nat. Commun.* **2**, 218 (2011)
12. L.A. Krivitsky, J.J. Wang, Z. Wang, B. Luk'yanchuk, Locomotion of microspheres for super-resolution imaging. *Sci. Rep.* **3**, 3501 (2013)
13. J. Aizpurua, P. Hanarp, D.S. Sutherland, M. Käll, Garnett W. Bryant, F.J. García de Abajo, Optical properties of gold nanorings. *Phys. Rev. Lett.* **90**, 057401 (2003)
14. Y. Sonnefraud, N. Verellen, H. Sobhani, G.A.E. Vandenbosch, V.V. Moshchalkov, P. Van Dorpe, P. Nordlander, S.A. Maier, Experimental realization of subradiant, superradiant, and fano resonances in ring/disk plasmonic nanocavities. *ACS Nano* **4**(3), 1664–1670 (2010)
15. R.L. Fork, O.E. Martinez, J.P. Gordon, Negative dispersion using pairs of prisms. *Opt. Lett.* **9**(5), 150–152 (1984)
16. M. Labardi, M. Zavelani-Rossi, D. Polli, G. Cerullo, M. Allegrini, S. De Silvestri, O. Svelto, Characterization of femtosecond light pulses coupled to hollow-pyramid near-field probes: localization in space and time. *App. Phys. Lett.* **86**(3), 031105 (2005)
17. M. Celebrano, P. Biagioni, M. Zavelani-Rossi, D. Polli, M. Labardi, M. Allegrini, M. Finazzi, L. Duò, G. Cerullo, Hollow-pyramid based scanning near-field optical microscope coupled to femtosecond pulses: a tool for nonlinear optics at the nanoscale. *Rev. Sci. Instrum.* **80**(3), 033704 (2009)